TOPOLOGICAL MATTER

Observation of chiral phonons

Hanyu Zhu,[1,2] Jun Yi,[1] Ming-Yang Li,[3] Jun Xiao,[1] Lifa Zhang,[4] Chih-Wen Yang,[3] Robert A. Kaindl,[2] Lain-Jong Li,[3] Yuan Wang,[1,2]* Xiang Zhang[1,2]*

Chirality reveals symmetry breaking of the fundamental interaction of elementary particles. In condensed matter, for example, the chirality of electrons governs many unconventional transport phenomena such as the quantum Hall effect. Here we show that phonons can exhibit intrinsic chirality in monolayer tungsten diselenide. The broken inversion symmetry of the lattice lifts the degeneracy of clockwise and counterclockwise phonon modes at the corners of the Brillouin zone. We identified the phonons by the intervalley transfer of holes through hole-phonon interactions during the indirect infrared absorption, and we confirmed their chirality by the infrared circular dichroism arising from pseudoangular momentum conservation. The chiral phonons are important for electron-phonon coupling in solids, phonon-driven topological states, and energy-efficient information processing.

Chirality is a fundamental property of an object not identical to its mirror image. For elementary and quasiparticles, it is an important quantum concept at the heart of modern physics. For example, the discovered handedness of neutrinos in electroweak interaction revolutionized our understanding of the universal parity conservation law. Chiral fermions with spin-momentum locking can emerge in solid-state systems such as the recently observed Weyl semimetals with inversion symmetry–breaking lattices (*1*). Electron chirality in graphene defined through pseudospin was found to cause distinctive transport properties such as unconventional Landau quantization and Klein tunneling (*2*, *3*). Meanwhile, electrons in monolayer transition metal dichalcogenides with broken inversion symmetry display optical helicity, which opens the field of valleytronics (*4*). The outstanding question is whether bosonic collective excitations such as phonons can attain chirality. Recently, the intrinsic chirality of phonons without applied external magnetic fields in an atomic lattice was predicted theoretically at the corners of the Brillouin zone of an asymmetric two-dimensional (2D) hexagonal lattice (*5*). Because of the threefold rotational symmetry of the crystal and the momentum vectors, the vibrational plane wave is composed of unidirectional atomic circular rotation. Because the phonons in the same valley have distinct energy levels, the rotation is not the superposition of linear modes, in contrast to the circular motion in nonchiral cases (*6*). The hypothetical chiral phonons are potentially important for the control of intervalley scattering (*7*, *8*), lattice modulation–driven electronic phase transitions (*9*, *10*) and topological states (*11*), as well as information carriers that can be robust against decoherence for solid-state quantum information applications (*12*).

Here we report the observation of intrinsic chiral phonons via transient infrared (IR) spectroscopy in the atomic lattice of monolayer WSe_2. A particle's angular momentum is calculated by the phase change under a rotational transformation. This definition can be extended for quasiparticles in solid lattices with discrete spatial symmetry, as long as the rotation is in the crystalline symmetry group (*13*). For an inversion symmetry–breaking 2D hexagonal lattice such as monolayer WSe_2 (Fig. 1A), phonons with well-defined pseudoangular momentum (PAM) are located at the Γ, K, and K′ points in the reciprocal space (*5*). Because the phonons inherit the threefold rotational (C_3) symmetry of the lattice, their function of motion must be C_3 invariant except for a phase difference (i.e., circular) (*14*). The K and K′ phonons are particularly notable because there is no reflection line that preserves both the lattice and their momentum (fig. S5). Therefore, the atomic rotation cannot be reversed without changing its momentum or energy. For example, if we attempt to reverse the rotational direction of the Se atoms in a longitudinal optical phonon LO(K) while keeping the relative phase determined by the $\mathbf{q} = \mathbf{K}$ momentum, the mode changes to a longitudinal acoustic phonon LA(K) that oscillates at a different frequency. Thus, unlike the Γ phonon, such a rotation cannot be decomposed into orthogonal linear vibrations with a $\pm\pi/2$ phase shift. On the other hand, to maintain the same mode, the relative phase must be reversed, resulting in a phonon at the K′ point.

We deduce the phonon PAM l for each mode from the phase change after counterclockwise 120° rotation: $\hat{C}_3(u_k) = e^{-i(2\pi/3)l}u_k$, where u_k is the function of atomic motion (fig. S6). Because LA(K) is always C_3 symmetric, it has $l = 0$; in contrast, LO(K) gains negative phase after rotation (becomes ahead of time) and thus $l = 1$. The K phonons with different PAM are completely nondegenerate because of the mass difference between W and Se. The lifting of degeneracy guarantees that each mode has a distinctive selection rule for the electron-phonon and optical scattering (table S1). These features differentiate the intrinsically chiral phonons from any previously investigated phonons where circular atomic motion results from superposing linear polarized eigenmodes (*6*, *15*, *16*). Chirality in the absence of an external magnetic flux is also distinguished from the magnetic field–induced split of degenerate superposition modes (*17*). Finally, both the physical origin and properties of the atomic chiral phonons are fundamentally different from previous phononic crystal–based chirality from geometric engineering or topological edge states (*18*–*20*).

We use an optical pump-probe technique to identify the chiral phonon by its scattering with holes (Fig. 1B and fig. S2). The linear momentum, PAM, and energy of the respective phonon modes are determined by characterizing all of the other particles involved in the intervalence band transition (IVBT) process (*14*). First, we inject holes at the K valley by a left–circularly polarized (LCP) optical pump pulse. The K valley–polarized hole relaxes to the valence band edge with initial linear momentum $\mathbf{p}_i = -\mathbf{K}$. It can transit to the K′ point ($\mathbf{p}_f = \mathbf{K}$) by emitting a K phonon ($\mathbf{q} = \mathbf{p}_i - \mathbf{p}_f = -2\mathbf{K} = \mathbf{K}$), but the intermediate state is virtual because the spin-conserving state has much higher energy due to large spin-orbit coupling. We then send an IR pulse to satisfy the energy conservation and place the hole in the spin-split band at K′. Because the hole states have zero PAM, the PAM of the phonon must be equal to the spin angular momentum of the absorbed IR photon. Therefore, the LCP pulse controls the creation of only LO(K) phonons. Eventually, we recognize the final spin-split state in the opposite valley by the energy and right circular polarization of its radiative decay. The selection rule of phonon creation will be identical if the hole first absorbs an IR photon, transits to an intermediate state within the valley, and then emits a phonon, as long as the final state is the same. The phonon annihilation is negligible because the population is very low for all phonon modes at the K or K′ points at a base temperature of 82 K. The selection is also not affected by a small momentum distribution of the initial and final holes (*14*) due to finite thermal energy or the strong many-body interaction (*21*). This is because, like the optical valley-selectivity, the contrast of electron-phonon coupling strength remains large in the vicinity of K and K′, even if the PAM is only defined on these points.

To determine the linear momentum of the involved phonon, we measure the linear momentum of the initial and final holes. Under circularly polarized pump excitation, the majority of holes maintain their linear momentum near the original valley, as shown by the positive helicity of the photoluminescence. The final linear momentum of the spin-split states is read out by the polarization of their luminescence at higher energy than the original pump photon (Fig. 2A). We measure the difference of luminescence with the same polarization as the pump light (I_{same})

[1]Nanoscale Science and Engineering Center, University of California, Berkeley, CA 94720, USA. [2]Materials Sciences Division, Lawrence Berkeley National Laboratory, Berkeley, CA 94720, USA. [3]Physical Sciences and Engineering Division, King Abdullah University of Science and Technology, Thuwal 23955-6900, Kingdom of Saudi Arabia. [4]Department of Physics, Nanjing Normal University, Nanjing, Jiangsu 210023, China.
*Corresponding author. Email: xzhang@me.berkeley.edu (X.Z.); yuanwang@berkeley.edu (Y.W.)

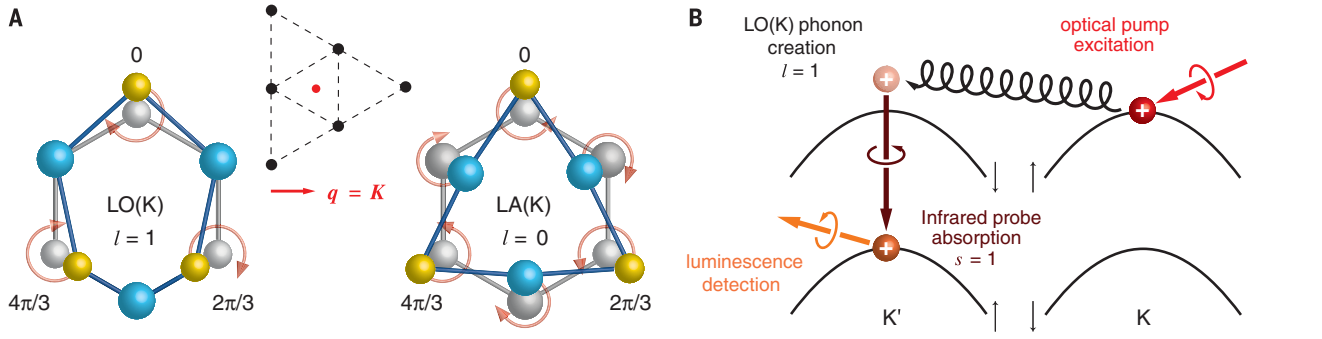

Fig. 1. Nondegenerate chiral phonons in monolayer WSe_2 and the selection rule of hole-phonon interactions. (**A**) The atomic motion of W and Se atoms (blue and yellow spheres, respectively) in the real space is intrinsically circular for the chiral phonons residing at the K point (red dot) in the reciprocal lattice (array of black dots), due to the threefold rotational symmetry. Because the momentum vector determines the relative phase of the Se motion, opposite rotations correspond to completely different modes. The two modes have distinct PAM with respect to the center of the hexagon. (**B**) In the intervalley optical transition of holes, the PAM of the K phonon is equal to the spin of the IR photon due to angular momentum conservation. A hole injected by the LCP optical pump moves from the K to the K′ valley through virtual scattering with a LO(K) phonon. Owing to the spin and energy mismatch, a real phonon is created only if the hole simultaneously absorbs an IR probe photon and transits to the spin-split state, which is signaled by the RCP luminescence.

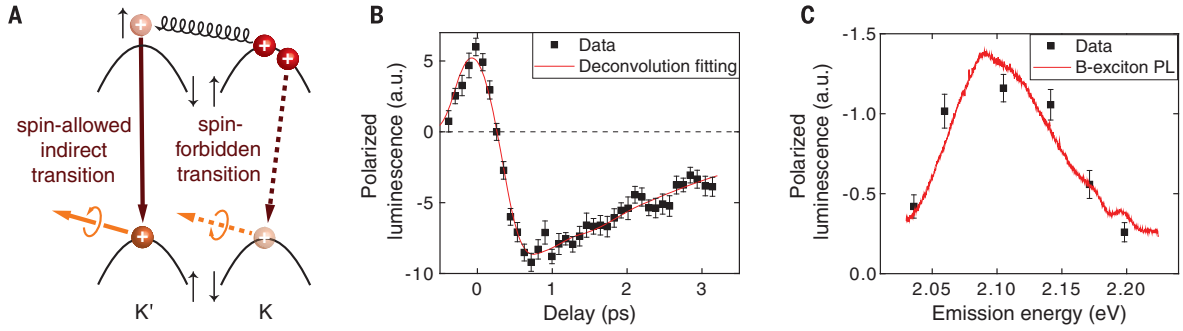

Fig. 2. Chiral phonon creation from the intervalley transition of holes measured by polarized luminescence. (**A**) The spin-allowed intervalley transition of holes from the K point creates a K phonon, yet the spin-forbidden transition within the same valley does not. The two processes are distinguished by the polarized luminescence signal. (**B**) The observed initial positive polarization indicates a spin-flipping transition of nonequilibrium holes, with a lifetime of ~0.2 ps. After that, the negative polarization shows a prevailing phonon-creating intervalley transition for valley-polarized holes, with a lifetime of ~2 ps at 82 K. The pump and probe energies are tuned to 1.97 and 0.51 eV, respectively, whereas the signal is integrated from 2.05 to 2.19 eV. (**C**) The spectrum of the polarized luminescence taken at τ = 0.8 ps agrees with the B-exciton photoluminescence (PL) and confirms its spin-split hole origin. The error bars in (B) and (C) indicate SE calculated from multiple measurements. a.u., arbitrary units.

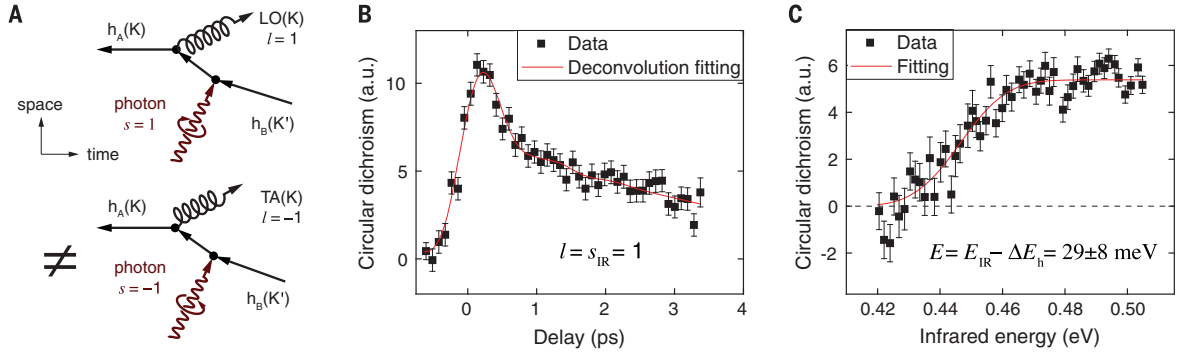

Fig. 3. Chirality of phonons measured by transient IR CD. (**A**) The phonons participating in the indirect optical transition are different for the LCP and RCP IR photons because of the conservation of linear and angular momentum. Their distinct electron-phonon scattering strengths dictate that the two processes have different amplitudes, leading to polarized IR absorption. $h_A(K)$, hole at the valence band edge of the K valley; $h_B(K')$, hole in the spin-split band of the K′ valley. (**B**) The measured CD at 82 K (black squares and red fitting curve) is positive for both the initial intravalley spin-flipping transition and the later intervalley phonon-creating transition. It not only proves the chirality of phonons but also indicates that the LO phonon process is dominant. (**C**) The spectrum of the transient CD acquired at τ = 0.8 ps shows a photonic energy threshold of 0.448 ± 0.002 eV. Its step shape is expected from the 2D excitonic density of states. Subtracting the energy difference between the initial and final hole states, a phonon energy of 29 ± 8 meV is deduced, in agreement with that of the LO mode. The error bars denote SE calculated from multiple measurements, and the threshold uncertainty indicates the SE of the fitting parameter.

and the opposite polarization (I_{oppo}) as a function of the probe delay time τ (Fig. 2B). We find that the polarized luminescence ($I_{same} - I_{oppo}$) is positive for $\tau < 0.2$ ps, indicating that the spin-flipping intravalley IVBT has a higher probability when the IR probe arrives immediately after the excitation of holes. This is because spin is not strictly conserved for optical transitions away from the high-symmetry points. However, the process is forbidden at the valley center with incident light perpendicular to the lattice plane, so its magnitude decays with a lifetime of 0.2 ps as the nonequilibrium carriers thermalize to the band edge (*22*, *23*). After that, the luminescence switches polarization as a result of the dominant spin-conserving intervalley IVBT. It shows that the majority of final holes have a linear momentum opposite that of the initial holes. The momentum must have been transferred to phonons instead of defects, as seen from the comparison of the second-order Raman scattering through the defect-assisted one-phonon process with that of the two-phonon process, which is an order of magnitude stronger (fig. S7). Directional intervalley transfer through electron-electron interactions (*24*) is excluded because the pump is not in resonance with the A exciton, and the signal is linearly proportional to the hole density (fig. S8). The exchange interaction reduces the polarization of the holes but should not create an opposite polarization (*25*). Finally, the depolarization plus the decay of the hole population yields a joint lifetime of ~2 ps for the polarized luminescence, in agreement with previous exciton studies (*26*). To further verify the nature of the final holes, we measure the polarized luminescence at different collection energies with τ = 0.8 ps. The emission spectra obtained with different IR photon energies are all close to the B-exciton photoluminescence (Fig. 2C and fig. S12), which proves that the emission is the radiative decay of a real state near the edge of the spin-split band, rather than a virtual state. Therefore, we use the luminescence from 2.05 to 2.19 eV to quantify the indirect IR absorption and the phonon creation.

The PAM of valley phonons is determined by measuring the polarization selection of the absorbed IR photon, resulting from the chiral electron-phonon interaction. With LCP excitation, the intervalley transition of holes from the K valley can either absorb an LCP IR photon to produce LO phonons or absorb a right–circularly polarized (RCP) IR photon to produce TA/A_1 phonons (Fig. 3A). We observe different IR absorption when the probe has the same polarization as the pump light (α_{same}) versus when it has the opposite polarization (α_{oppo}). This IR circular dichroism (CD = $\alpha_{same} - \alpha_{oppo}$) demonstrates that scattering cross sections of the two processes are not equal, owing to the difference of electron-phonon coupling strength. As shown in Fig. 3B, the CD at 82 K is always positive for valley-polarized holes. Because the holes have zero PAM regardless of valley index or spin-split bands, the angular momentum of the IR photon is transferred to either the spin or the phonon. The initial intravalley IVBT produces positive CD because the electronic spin flips from −1/2 in the spin-split band to +1/2 at the valence band edge at the K point. However, this contribution decays fast as a function of IR delay in accordance with Fig. 2B. Thus, the intervalley phonon-creating transition is the dominant source of positive CD for $\tau \geq 0.8$ ps. It indicates that the LO branch contributes most to the indirect IR absorption. For nonchiral systems, although photons with opposite circular polarization may interact with different particles, the probabilities are always equal. Therefore, the CD is the signature of intrinsic phonon chirality.

The energy of this phonon mode is measured according to energy conservation: The energy sum of the incoming particles, the IR photon, and the initial holes must be equal to that of the outgoing particles, the chiral phonon, and the final holes (*14*). We observe that the CD spectrum at τ = 0.8 ps (Fig. 3C) is a step function with a clear threshold near 0.448 ± 0.002 eV, broadened by the spectral width of the IR pulse. The shape corresponds to a transition from a hole at the valence edge to a band with parabolic dispersion in two dimensions (fig. S9). This value is distinguished from either the intra-excitonic transition (*27*) or the exciton dissociation energy (*21*). Next, we find that the ground-state configuration of the initial holes is the dark A trion at E_i = 1.671 ± 0.006 eV (fig. S11) (*28*) based on the dominant bright A-trion photoluminescence (fig. S1). We verify that the dark trions are near thermal equilibrium because the IR spectrum is very different from that of nonequilibrium carriers with excessive energy at τ = 0 ps (fig. S10). The final state is the bright B trion at E_f = 2.090 ± 0.005 eV, as measured through its emission (fig. S12). Summarizing these values, we deduce the phonon energy $E_{phonon} = E_{photon} + E_i - E_f = 29 \pm 8$ meV, in agreement with the first-principles calculation and the Raman spectrum for the LO(K) mode (figs. S7 and S9). The uncertainty may be reduced in the future by improving the uniformity of the sample and the spectral resolution of the B-exciton emission. Better spectroscopy will also potentially reveal details about the chiral phonon-exciton coupling—such as the contribution from LA phonons and the various pathways of the indirect transition—that are not resolvable with the current signal-to-noise ratio.

Our findings of chiral phonons are fundamentally important for potential experimental tests of quantum theories with chiral bosons (*29*) in the solid state. Our work also provides a possible route for controlling valley and spin through electron-phonon scattering and strong spin-phonon interactions (*16*). Furthermore, the lifting of degeneracy by chirality offers robust PAM information against decoherence and long-range perturbation and offers a new degree of freedom to the design and implementation of phononic circuitry (*30*) at the atomic scale without magnetic fields.

REFERENCES AND NOTES

1. M. Z. Hasan, S.-Y. Xu, I. Belopolski, S.-M. Huang, *Annu. Rev. Condens. Matter Phys.* **8**, 289–309 (2017).
2. F. D. M. Haldane, *Phys. Rev. Lett.* **61**, 2015–2018 (1988).
3. S. Das Sarma, S. Adam, E. H. Hwang, E. Rossi, *Rev. Mod. Phys.* **83**, 407–470 (2011).
4. J. R. Schaibley *et al.*, *Nat. Rev. Mater.* **1**, 16055 (2016).
5. L. Zhang, Q. Niu, *Phys. Rev. Lett.* **115**, 115502 (2015).
6. H. Katsuki *et al.*, *Nat. Commun.* **4**, 3801 (2013).
7. H. Zeng, J. Dai, W. Yao, D. Xiao, X. Cui, *Nat. Nanotechnol.* **7**, 490–493 (2012).
8. B. R. Carvalho *et al.*, *Nat. Commun.* **8**, 14670 (2017).
9. M. Rini *et al.*, *Nature* **449**, 72–74 (2007).
10. M. Först, R. Mankowsky, A. Cavalleri, *Acc. Chem. Res.* **48**, 380–387 (2015).
11. G. Jotzu *et al.*, *Nature* **515**, 237–240 (2014).
12. K. C. Lee *et al.*, *Science* **334**, 1253–1256 (2011).
13. R. C. Johnson, *Phys. Lett. B* **114**, 147–151 (1982).
14. Materials, methods, and additional information are available as supplementary materials.
15. S.-Y. Chen, C. Zheng, M. S. Fuhrer, J. Yan, *Nano Lett.* **15**, 2526–2532 (2015).
16. T. F. Nova *et al.*, *Nat. Phys.* **13**, 132–136 (2017).
17. G. Schaack, *J. Phys. C* **9**, L297–L301 (1976).
18. A. Spadoni, M. Ruzzene, S. Gonella, F. Scarpa, *Wave Motion* **46**, 435–450 (2009).
19. R. Süsstrunk, S. D. Huber, *Science* **349**, 47–50 (2015).
20. C. Brendel, V. Peano, O. J. Painter, F. Marquardt, *Proc. Natl. Acad. Sci. U.S.A.* **114**, E3390–E3395 (2017).
21. T. Low *et al.*, *Nat. Mater.* **16**, 182–194 (2017).
22. F. Ceballos, Q. Cui, M. Z. Bellus, H. Zhao, *Nanoscale* **8**, 11681–11688 (2016).
23. P. Steinleitner *et al.*, *Nano Lett.* **17**, 1455–1460 (2017).
24. M. Manca *et al.*, *Nat. Commun.* **8**, 14927 (2017).
25. T. Yu, M. W. Wu, *Phys. Rev. B* **89**, 205303 (2014).
26. T. Yan, J. Ye, X. Qiao, P. Tan, X. Zhang, *Phys. Chem. Chem. Phys.* **19**, 3176–3181 (2017).
27. C. Poellmann *et al.*, *Nat. Mater.* **14**, 889–893 (2015).
28. X.-X. Zhang *et al.*, *Nat. Nanotechnol.* **12**, 883–888 (2017).
29. M. M. H. Barreira, C. Wotzasek, *Phys. Rev. D Part. Fields* **45**, 1410–1415 (1992).
30. N. Li *et al.*, *Rev. Mod. Phys.* **84**, 1045–1066 (2012).

ACKNOWLEDGMENTS

We thank F. Wang and Q. Niu for helpful discussions. This work was primarily supported by the U.S. Department of Energy, Office of Science, Basic Energy Sciences, Materials Sciences and Engineering Division under contract no. DE-AC02-05-CH11231 within the van der Waals Heterostructures program (KCWF16) for sample preparation and theory and data analysis, and within the Subwavelength Metamaterials Program (KC12XZ) for optical design and measurement. R.A.K. was supported under the same contract within the Ultrafast Materials Science program (KC2203) for mid-IR frequency conversion. J.Y. acknowledges a scholarship from the China Scholarship Council (CSC) under grant no. 201606310094. L.Z. thanks M. Gao for helpful calculation and discussion and acknowledges support from the National Natural Science Foundation of China (grant no. 11574154). L.-J.L. acknowledges support from the King Abdullah University of Science and Technology through a Competitive Research Grant (CRG5) for monolayer WSe_2 synthesis. All data needed to evaluate the conclusions in the paper are present in the paper and the supplementary materials.

SUPPLEMENTARY MATERIALS

www.sciencemag.org/content/359/6375/579/suppl/DC1
Materials and Methods
Figs. S1 to S12
Table S1
References (*31*–*46*)
Movies S1 and S2

20 October 2017; accepted 19 December 2017
10.1126/science.aar2711

Science

Observation of chiral phonons

Hanyu Zhu, Jun Yi, Ming-Yang Li, Jun Xiao, Lifa Zhang, Chih-Wen Yang, Robert A. Kaindl, Lain-Jong Li, Yuan Wang and Xiang Zhang

Science **359** (6375), 579-582.
DOI: 10.1126/science.aar2711

A phonon merry-go-round

Chirality is associated with the breaking of symmetry, often described as left- or right-handed behavior. Such asymmetry can be seen, for example, in the electronic responses of particular materials or the reactions between particular chemical species. Zhu *et al.* observed a chiral phonon mode in a monolayer of the transition metal dichalcogenide WSe_2, detected spectroscopically as the circular dichroism of the phonon-assisted transition of holes. Phonon chirality could be used to control the electron-phonon coupling and/or the phonon-driven topological states of solids.

Science, this issue p. 579